



This is a repository copy of *Assessment of Post-Restrained Shrinkage Mechanical Properties of Concrete*.

White Rose Research Online URL for this paper:  
<http://eprints.whiterose.ac.uk/100388/>

Version: Accepted Version

---

**Article:**

Younis, K.H. and Pilakoutas, K. (2016) Assessment of Post-Restrained Shrinkage Mechanical Properties of Concrete. *ACI Materials Journal*, 113 (3). pp. 267-276. ISSN 0889-325X

---

**Reuse**

Unless indicated otherwise, fulltext items are protected by copyright with all rights reserved. The copyright exception in section 29 of the Copyright, Designs and Patents Act 1988 allows the making of a single copy solely for the purpose of non-commercial research or private study within the limits of fair dealing. The publisher or other rights-holder may allow further reproduction and re-use of this version - refer to the White Rose Research Online record for this item. Where records identify the publisher as the copyright holder, users can verify any specific terms of use on the publisher's website.

**Takedown**

If you consider content in White Rose Research Online to be in breach of UK law, please notify us by emailing [eprints@whiterose.ac.uk](mailto:eprints@whiterose.ac.uk) including the URL of the record and the reason for the withdrawal request.



[eprints@whiterose.ac.uk](mailto:eprints@whiterose.ac.uk)  
<https://eprints.whiterose.ac.uk/>

## **Assessment of post-restrained shrinkage mechanical properties of concrete**

Khaleel H. Younis, Kypros Pilakoutas

**Khaleel H. Younis**, is a research Civil Engineer and a Lecturer of concrete technology at Erbil Polytechnic University, Erbil, Kurdistan, Iraq. He received his BSc and MSc from Al-Mustansiriya University, Baghdad, Iraq and recently completed his PhD at The University of Sheffield, Sheffield, UK.

**Kypros Pilakoutas**, is a Professor of Construction Innovation in the Department of Civil and Structural Engineering at The University of Sheffield. He received his BSc (in 1984) and PhD (in 1990) from Imperial College, London, UK. He is a member of fib task group 9.3 (Composites for construction) and the leader of several EU funded multi-partner projects including "Anagennisi". His research interests include structural concrete behaviour, earthquake engineering, composites for construction and construction innovation.

### **ABSTRACT**

Restrained shrinkage induced cracks can cause issues with serviceability, structural integrity and durability in concrete, but are difficult to predict. This paper proposes a simple, and economical test rig for restrained shrinkage and associated procedures to assess the post-shrinkage mechanical properties (compressive and flexural strength) of concrete. The results show that the restraining factor of the proposed rig is dependent on the time and the stiffness of the concrete. Results of residual mechanical properties show that restrained shrinkage induced cracks can affect the mechanical behaviour (flexural and compressive strength and stiffness) of concrete by up to 21%.

Keywords: Restrained shrinkage; Free shrinkage; Post-restrained shrinkage properties; Shrinkage cracks.

## INTRODUCTION

Due to chemical, thermal and physical changes, concrete develops unavoidable complex volume changes which lead to time-dependent internally induced deformations. Drying and autogenous shrinkage are the results of such changes. Restraint against these internally induced deformations result in stress development <sup>1</sup> that can lead to cracking if such stresses exceed the tensile strength of concrete <sup>2</sup>. Cracks, induced by restrained shrinkage, can cause issues with serviceability and structural integrity. Shrinkage induced cracks can also compromise durability by affecting properties such as permeability, diffusivity and sorptivity, enhancing the ingress of detrimental substances, freeze-thaw damage, corrosion of steel reinforcement and spalling. All these premature deteriorations and structural deficiencies often occur prior to the application of external loads. Therefore, the excessive development of concrete cracks should be controlled at early ages<sup>3,4</sup>.

If there is no restraint against volume changes, no significant cracks are expected to develop. However, all concrete elements are practically restrained to some degree, since some internal or external restraint always exists<sup>5</sup>. External restraint may result from supporting elements (e.g. walls and columns), contact with adjacent elements and, in the case of concrete pavements or slabs on grade, applied loads and base friction <sup>1,6</sup>. Internal restraint sources comprise of aggregates and reinforcement<sup>7</sup>. Internal restraint can also be caused by non-uniform drying shrinkage, which is usually caused by either moisture or temperature gradients <sup>1</sup>.

The best way to mitigate the effect of shrinkage deformations is to prevent the loss of moisture and protect the concrete from rapid cooling. Nonetheless, from a practical prospective, the complete elimination of internal deformations is impossible. Hence, it is important to find ways of quantifying restrained strains and associated stresses so as to account for them at the design process.

Restrained shrinkage is a major design issue for concrete pavements. Technical report No.34 of Concrete Society <sup>8</sup> identifies the need for shrinkage induced stresses to be included in the design procedures of concrete industrial floors and slabs on grade. However, due to lack of advanced

knowledge and design models, in the calculation of the hogging moment capacity of the slabs, a fixed value of restrained flexural tensile stress is subtracted from the flexural tensile strength of the concrete irrespective of the material properties and geometry of the element. This restrained tensile stress is calculated using free shrinkage strains (stress = free shrinkage strains  $\times$  restraint factor  $\times$  effective elastic modulus). Nonetheless, TR34 does identify that the interaction between shrinkage induced stresses and those caused by external loading need further research.

Free shrinkage tests can provide information on the shrinkage behaviour of different concrete mixtures, based on the environmental conditions, and size and shape of concrete elements being assessed. However, such tests cannot provide information on the post-cracking behaviour of concrete under restrained conditions<sup>9-12</sup>. Restrained shrinkage tests help in the assessment of cracking tendencies and the ability of concrete to withstand shrinkage induced tensile stresses<sup>2,13,14</sup>.

There is no standardized test to assess the post shrinkage behaviour of concrete under restrained conditions<sup>9,11,13</sup>. However, both the American Association of State Highway and Transportation Officials (AASHTO in 2008) and the American Society for Testing and Materials (ASTM in 2004) adopted the ring test<sup>15</sup> (see Fig. 1) as a standard test for restrained drying shrinkage. Simplicity and versatility are the main features of this test. For a given drying environment, the ring test can provide information of the age of the concrete at cracking, the width of the cracks, and the rate of crack width increase with time. This information can be used to compare the cracking sensitivity of different mixtures or to assess the efficiency of materials such as fibres in controlling crack width<sup>1,12</sup>. However, the test has the following drawbacks:

1. The test does not simulate and cannot predict concrete cracking in actual service life, and rather reflects the relative cracking tendency of concrete mixtures<sup>12,16,17</sup>,
2. The strains used to calculate the elastic stresses are not measured directly from the concrete; instead they are measured on the outer face of the steel ring (see Fig. 1), assuming a linear stress distribution throughout the steel ring<sup>1</sup>,

3. The test cannot quantify the residual strength of cracked concrete.

Several other test methods for restrained drying shrinkage have been proposed<sup>18</sup>. These can be classified by the shape of the specimen into plate or linear tests<sup>19</sup>, with the former providing biaxial restraint, whereas the latter providing uniaxial restraint. In linear tests, the ideal configuration to provide full restraint against shrinkage strains is to rigidly fix the concrete specimen at its ends (see Fig. 2a). This is practically impossible since an infinitely stiff reaction frame and fixity/gripping system is required. Therefore, other more practical solutions have been attempted using passive (Fig. 2b) and active restraint control (Fig. 2c)<sup>18</sup>.

In practice narrow slabs, suffer more from shrinkage cracking than square slabs of the same length. This means that the more convenient uniaxial restraint tests are expected to lead to conservative results. In linear-passive tests (e.g. RILEM test)<sup>20</sup>, the restraint is provided by stiff steel sections or by embedding restraining steel reinforcement bars in the specimen ends (the bar being debonded in the middle part only)<sup>2,21,22</sup>. Passive tests usually provide partial, often unknown, level of restraint. In linear-active tests, one end is fixed (restrained) and the other is left free<sup>18</sup>. The free end is either manually adjusted using a screw<sup>23,24</sup> or using an actuator<sup>25</sup>, but these can be fully actively computer controlled to simulate full fixity<sup>14</sup> (provided the gripping system is rigid). This method has the merit of quantifying tensile creep strains and is used by others<sup>13,26</sup>. Different mechanisms can be used to grip the ends of the concrete specimen. These mechanisms include:

- 1- bolt anchors using a number of steel threaded bars at the end of the concrete specimen (see Fig. 2d)<sup>12,27</sup>,
- 2- lateral clamping utilizing steel plates and threaded bars at the ends of the specimen to clamp the ends against the reaction frame (see Fig. 2e)<sup>11</sup>,
- 3- fixity using enlarged end specimen to fit into steel grip reaction at the ends (e.g. dog-bone, see Fig. 2f)<sup>14,20</sup>,
- 4- epoxy to bond the concrete specimen to end supports and the reaction rig<sup>28</sup>.

From linear tests, a variety of concrete properties can be obtained such as: shrinkage (drying and autogenous) strain and stress, age of cracking, crack width, creep strain of concrete, development of tensile stress with time and degree of restraint. From a practical point of view when many parameters are needed to be examined, the setting up of such tests and their instrumentation can be complicated and expensive. Automatic strain measurements are also difficult since cracking positions are not known in advance. The small dimensions of the specimens used in some of these tests, mainly to reduce costs, is also another issue, since they limit the use of normal size coarse aggregates. In fact, in some of these tests no coarse aggregate is used at all<sup>17</sup>. Another issue to consider is how to dismount the concrete specimen at the end of the drying exposure time without destroying it. As a result of these difficulties, such tests are avoided in common quality control testing and large-scale parametric study investigations<sup>1,29</sup>.

The impact of shrinkage induced cracks due to external restraints on the mechanical properties (compressive strength, flexural strength and stiffness) of concrete is not well studied and in fact, there is no standard experimental procedure to quantify the effect of shrinkage cracks on these properties. Nonetheless, these are the most important properties needed to design restrained concrete elements, such as slabs on grade. For this reason, the current study attempts to develop a simple and economical test rig for restrained shrinkage and a procedure that can quantify the post-shrinkage residual mechanical properties of concrete.

The proposed rig is presented next followed by details of the experimental procedure used to evaluate its effectiveness. These are followed by a critical discussion of the results and recommendations for improvements.

## **RESEARCH SIGNIFICANCE**

Cracking due to restrained shrinkage is of major concern for both serviceability and durability of concrete. Quantifying restrained strains and associated stresses are crucial to account during the design process as this helps to include the effect of restrained shrinkage induced cracks

on the properties of concrete which are usually used in the design process of concrete elements. The absence of a standard or a practical test to quantify the effect of shrinkage induced cracks on the mechanical properties of concrete limits the understanding of what happens after shrinkage cracking. This study is an attempt to develop a new restrained shrinkage test and a procedure to quantify the post-shrinkage mechanical properties of concrete.

## **PROPOSED RESTRAINED SHRINKAGE TEST RIG**

For a restrained shrinkage test, a suitable starting point was found in the configuration used by Weiss et al, 1998 who developed a test method for assessing the shrinkage cracking potential of normal and high strength concrete (with and without fibres) for pavement applications (see Fig. 3). The depth of the section used by Weiss et al was only 25 mm (1 in). However, a deeper specimen is required to: 1) enable the use of coarse aggregate 20 mm (0.75 in), and 2) to allow the specimens to be used for flexural tests (e.g the ASTM C1609). However, the increase in depth means a bigger concrete section that requires a larger restraining force and thus more effective end restraint conditions to provide restraint against shrinkage strains. Furthermore, the test-rig should allow the demoulding of the concrete specimens at an early stage and the demounting at the end of the restraining period.

Fig. 4 shows the general layout of the developed rig. The new set up consists of a reaction beam (I-section) with sufficient dimensions (flange width=168 mm (6.6 in), thickness of web= thickness of flange = 10 mm (0.4 in)) to provide enough stiffness (at least 4 times the stiffness of hardened concrete) to resist axial shortening. The reaction beam is 1m long with its upper flange polished to provide a smooth and slippery surface to ensure that the restraint only develops at the ends. Two L-shaped steel supports are bolted to the flange to provide restraint at the ends of the concrete specimen. The concrete ends are fixed to the steel angles by four bolts at each end and split at their ends to increase their ability to grip the concrete. These bolts will enable easy dismounting of the concrete specimen after the completion of the drying period.

The concrete section is reduced from 130 mm (5.11 in) to 100 mm (4 in) away from the supports to avoid crack formation at the anchorage zone. Furthermore, to achieve a more uniform drying condition around the concrete section, removable framework is used to separate the bottom of the concrete surface from the steel surface. To achieve this, a timber plate (15 mm (0.6 in) thick and 530 mm (21.2 in) long with curved ends) cut into three parts with a wedge at the mid-section is used to ensure easy removal (24 h) after casting the concrete specimen. A similar plate is used on the top face to increase the cross section of the concrete at the ends (anchor zone) and obtain a uniform shape of the concrete specimen as can be seen in Fig.4. The proposed rig was used in trial tests described below to assess its effectiveness in quantifying the post-shrinkage residual mechanical properties of concrete.

## **MATERIALS AND EXPERIMENTAL PROCEDURES**

### **Materials and specimen preparation**

Portland Cement CEM I 52.5 N, meeting the requirements of BS EN 197-1<sup>30</sup> was used in this research. The fine aggregate used in this study was sand with a maximum size of 5 mm (0.2 in). The coarse aggregate was river aggregate with maximum size of 20 mm (0.75 in).

The mix proportion was cement: water: sand: gravel= 390:176:560:1111 (kg/m<sup>3</sup>) (657:297:944:69.4 lb/yd<sup>3</sup>) with w/c ratio 0.45.

In the moulds (prisms for free and restrained shrinkage and cubes), the concrete was cast in three layers, and each layer was compacted using the vibrating table. For the restrained shrinkage specimen, the compaction was undertaken by placing the I-section on the vibrating table and the top plate was placed immediately after casting. The specimens were then covered by plastic sheet and allowed to cure for 24 hours before being demoulded. A slightly shorter 500 mm long (20 in) control prism was stored in water and a second control prism 750×100×100 mm (30×4×4 in) for free shrinkage test was stored next to the restrained specimen at 22 ± 2 °C and RH of 45 ± 5 %.

Furthermore, 15 cubes of 100 mm (4 in) were cast to determine the compressive strength at different times.

Immediately after demoulding the prisms prepared for free and restrained shrinkage tests, Demec gauge points were fixed to the concrete surface at 50 mm (2 in) spacing (see Fig. 5) using a rapid-hardening adhesive on the top and side surfaces.

## Tests

### Free and Restrained Shrinkage

Three Demec gauges were used to measure strains having lengths 50, 100 and 300 mm (2, 4 and 12 in) and precision of 20, 16 and 5.2  $\mu\epsilon$  (20, 16 and 5.2  $\times 10^{-6}$  in/in). The first shrinkage strains were measured at 24 h (soon after the adhesive hardened) and at 24 h intervals for the first week, followed by measurements at 10, 14, 21 and 28 days. Two or three readings were taken for each gauge length, and the average values calculated.

According to ACI 207.2R-95<sup>31</sup> the degree of restraint or restraint factor (RF) is given as the ratio of actual stress induced by the restrained volume change to the stress which would develop if the specimen was fully restrained. In other words, it is a ratio between the amount of strain that is restrained to the free shrinkage strain<sup>32</sup>. Assuming the modulus of elasticity is constant, equation 1 can be used to calculate the RF:

$$RF = \frac{\epsilon_R}{\epsilon_{free}} \quad (1)$$

where:

$\epsilon_R$  Restrained shrinkage strain= shrinkage strain measured on the free specimen - shrinkage strain measured on the restrained specimen.

$\epsilon_{free}$  Free shrinkage strain (strain measured on the free specimen).

## CRACK DETECTION

Regular daily checks for cracks were performed using an optical microscope with a magnification factor of 40x and a precision of 20  $\mu\text{m}$  ( $8 \times 10^{-4}$  in) and a digital microscope with a magnification up to 200x and a precision of 10  $\mu\text{m}$  ( $4 \times 10^{-4}$  in). The crack width reported here is the crack opening at its widest, normally at the edge of the specimen.

There is no clear definition of what is a microcrack in the literature. RILEM committee TC-122-MLC on "Microcracking and life time performance of concrete", (cited in Idiart, 2009<sup>33</sup>) uses width of less than 10  $\mu\text{m}$  ( $4 \times 10^{-4}$  in) to define microcracks. Others<sup>33-35</sup> adopt 50  $\mu\text{m}$  ( $20 \times 10^{-4}$  in). In this study 20  $\mu\text{m}$  ( $8 \times 10^{-4}$  in) or less was used to define the microcracks, as it was found that cracks with width larger than 20  $\mu\text{m}$  ( $8 \times 10^{-4}$  in) are visible to the naked eye when properly illuminated.

#### Loss of Mass (loss of moisture)

The loss of mass for the free shrinkage specimen was determined using a balance with the precision of 0.1 g (0.0002 lb). The first reading, which is considered as the initial mass, was measured at 24 h, after the Demec points were bonded. Thereafter, the readings were obtained at the same time intervals as for the free shrinkage measurements.

#### Compressive Strength

The compressive strength was obtained at 1, 3, 7, 28 and 75 days using the 100mm cubes (4 in) and BS EN 12390-3<sup>36</sup>. The compressive strength was also obtained from the two prisms tested in bending, by following the recommendations of BS 1881-119<sup>37</sup>.

#### 3.2.5 Flexural tests

All prisms (prisms cured in water and prisms exposed to shrinkage) were tested in four-point loading over a length of 300 mm following the recommendations of the ASTM C1609M-12<sup>38</sup> using a universal testing machine in displacement control. A yoke was used to mount the deflection transducers and to eliminate errors from support displacement and torsion. The central deflections were determined from the average of two linear variable displacement transducers (LVDTs) placed on opposite sides of the specimen. From the load versus-deflection curve, the flexural strength and

stiffness (flexural modulus of elasticity) were calculated. Equation 2 was used to determine the flexural modulus of elasticity  $E_{flex}$  (GPa) from the stiffness, based on the theory of classical elasticity.

$$E_{flex} \text{ (GPa)} = \frac{23P}{1296\delta} \cdot \frac{L^3}{I} \left[ 1 + \frac{216}{115} \left( \frac{h}{L} \right)^2 (1 + \nu) \right] \quad (2)$$

where :

$P/\delta$  is the slope of the linear elastic part of the load-deflection curve (kN/mm);  $L$  is the supported span of the prism (mm);  $I$  is the second moment of area of the cross-section ( $\text{mm}^4$ );  $b$  is the width of the cross-section (mm);  $h$  is the height of the cross-section (mm); and  $\nu$  is the Poisson's ratio. The flexural elastic modulus of concrete  $E_{fmax}$  was determined as the maximum value of  $E_{flex}$  in the range of 30% to 60% of the ultimate bending load (linear part of the load-deflection curve where  $E_{flex}$  is almost constant).

## **EXPERIMENTAL RESULTS AND DISCUSSION**

### **Free shrinkage strains**

Fig. 6 and Fig. 7 show the results of free shrinkage strain using the three gauge lengths 50, 100 and 300 mm (2, 4 and 12in) taken from the side and top, respectively. As expected the shrinkage rate is high at the early age slowing down with time; the shrinkage strain after one week was almost 40% of that measured at 75 days. Fig. 6 and 7, also show that the measured strains using the different gauge lengths are similar.

The shrinkage strains measured on the top surface of the concrete specimen are slightly higher than those measured on the side surface. This may be due to concrete bleeding which usually happens at the top (troweled) surface altering the microstructure of this surface and possibly resulting in slightly higher porosity which in turn causes more shrinkage. Furthermore, concrete is better compacted at bigger depths resulting in more dense concrete, which tends to shrink less.

## **Restrained shrinkage strains, degree of restraint and characterisation of cracks**

The shrinkage strains measured on the side of the restrained specimen are shown in Fig. 8 for 50 mm (2 in) gauge length and in Fig. 9 for the 300 mm (12 in) gauge length. Fig. 8 represents the average shrinkage strains that occurred over time for 14 individual distances. The development of large strains on the restrained sample indicates that the developed rig only provides partial restraint.

Fig. 10 shows that the RF was 64% on the first day. After 5 days of drying, it decreased to almost 46%. Thereafter, it decreased to 21% at 28 days and around 14% at 75 days. It should be noted that microcracks occurring at the ends of the sample also reduce the restraint efficiency, resulting in a lower degree of apparent restraint.

After 1 day of drying, the first microcracks were detected at several positions using the digital micro-scope. A slight reduction in the shrinkage strain (restrained specimen) was observed (see Fig. 8 and 9) after 7 days of drying, though no visible cracks were observed. Such a reduction in the shrinkage strains measured on the restrained specimen can only be due to cracks developing further. After 9 days of drying few visible cracks were recorded at the top edges of the specimen. The width of the visible cracks were in the range of (0.025-0.035) mm when first detected. Similar observations were reported by Grzybowski and Shah<sup>9</sup> (drying conditions: temperature = 20 °C and RH = 40%) Weiss et al<sup>11</sup> (drying conditions: temperature = 23 °C and RH = 50%) during the monitoring of restrained concrete specimens (ring type), as they noticed a decrease in the strain measured on the steel ring prior to the detection of cracks. Many microcracks were detected by the microscopes, but only 10 visible cracks were observed. Details on the visible cracks at 75 days are summarized in Table 1.

Crack growth was very slow. This is evident by comparing the initial and the final crack width of the detected cracks (see Table 1). The maximum crack width measured was 55µm ( $22 \times 10^{-4}$  in) (crack 1) at the age of 75 days. Although visible cracks developed on both sides of the

restrained specimen, none of them propagated and turned into a through crack. This can be attributed to the following reasons: a- the cracks that formed at the ends of the specimen may have reduced the degree of restraint, b- the slow rate of shrinkage strain development after the first week of exposure, c- the effect of tensile creep which can serve to relax shrinkage stresses. The distribution of the cracks at age 75 day is shown in Fig. 11.

Microcracks were also observed on the surfaces of the free shrinkage specimens. These randomly distributed discontinuous cracks had a net shape and developed at different areas on the surfaces of the concrete. The larger crack width at day 75 was 0.02 mm ( $20 \times 10^{-4}$  in). The main cause of such cracks is internal restraint (differential drying) caused by moisture gradient.

### **Mass loss**

Mass loss versus time is shown in Fig. 12a. It can be seen that mass loss is faster at the early stages, behaving in the same way as shrinkage strain. Nonetheless, when shrinkage strain is plotted against mass loss (see Fig. 12b) a different trend can be seen as the initial rate of mass loss is much faster than the shrinkage strain rate. This may be due to the fact that during the first week, though moisture is lost at a higher rate, this moisture is being lost from coarse pores, resulting in relatively low shrinkage due to low capillary pressures. With further drying, finer pores start to lose moisture, causing higher capillary pressure, thus resulting in higher shrinkage for a smaller mass loss.

### **Effect of strain loss on RF and cracking development**

It is evident from the recorded strain loss on the prisms that the rig only offers partial restraint. Strain loss may occur due to deformations of the restraining beam (bending and contraction) and the end supports (L-shape) caused by the tensile force applied by the restrained concrete (see Fig. 13). Finite element elastic analysis (see Fig. 14) was performed to calculate these strain losses. The finite element analysis was undertaken using Abaqus/CAE software (version 6.9-1). A deformable three dimensions element was utilized. The analysis shows that the greatest part of strain loss is caused by the deformation of the end supports. For example, the magnitude of the

expected tensile force resulting from a  $100 \mu\epsilon$  ( $100 \times 10^{-6}$  in/in) shrinkage strain ( $E_c = 26$  GPa, 3770 ksi), will lead to a strain loss of  $20 \mu\epsilon$  ( $20 \times 10^{-6}$  in/in) due to shortening and  $43 \mu\epsilon$  ( $43 \times 10^{-6}$  in/in) due to beam bending. The same force would also pull-in the end supports with a corresponding strain loss of  $200 \mu\epsilon$  ( $200 \times 10^{-6}$  in/in). Part of these elastic strain losses will be counteracted by the creep effect.

To estimate the variation of the RF over time and compare it with the apparent (measured) RF (Fig. 10), the ratio between the stiffness of the concrete and the rig must be known. This can be determined by using equilibrium and compatibility conditions. Equation 3 represents the equilibrium equation of the forces that develop in the concrete (tensile force,  $F_c$  or  $F_{rig}$ ) due to restrained shrinkage.

$$F_c = F_{rig} \quad (3)$$

$$E_c A_c \epsilon_c = E_{rig} A_{rig} \epsilon_{rig} \quad (4)$$

where:

$E_c, E_{rig}$  = elastic modulus of concrete and rig, respectively.

$A_c, A_{rig}$  = cross-sectional area of concrete and rig, respectively .

$\epsilon_c$  = restrained shrinkage strain.

$\epsilon_{rig}$  = strain developed in the rig due to shrinkage induced forces.

$$\frac{E_c A_c}{E_{rig} A_{rig}} = \frac{\epsilon_{rig}}{\epsilon_c} \quad (5)$$

if 
$$K = \frac{E_c A_c}{E_{rig} A_{rig}} \quad (6)$$

then 
$$K = \frac{\epsilon_{rig}}{\epsilon_c} \quad (7)$$

Hence, the stiffness ratio (K) between the concrete and the restraining rig is equal to the ratio of the restrained shrinkage strain of concrete ( $\epsilon_c$  or  $\epsilon_R$ ), which results in developing a tensile

force in the concrete, to the strain of the rig (strain loss,  $\varepsilon_{\text{rig}}$ ) caused by the same force (see Fig. 15).

From Fig. 15, the strain compatibility equation can be developed as follows:

$$\varepsilon_c + \varepsilon_{\text{rig}} = \varepsilon_{\text{free}} \quad (8)$$

From equation 5:

$$\varepsilon_{\text{rig}} = K\varepsilon_c \quad (9)$$

$$\text{Then: } \varepsilon_c + K\varepsilon_c = \varepsilon_{\text{free}} \quad (10)$$

$$\varepsilon_c \text{ or } \varepsilon_R = \frac{\varepsilon_{\text{free}}}{1 + K} \quad (11)$$

$$\text{Since, } \text{RF} = \frac{\varepsilon_R}{\varepsilon_{\text{free}}} \quad (\text{eq. 1})$$

$$\text{Then, the estimated RF is: } \text{RF} = \frac{1}{1 + K} \quad (12)$$

Equation 12 can be used to assess the effect of  $E_c$  on the estimated RF. By using the same previous example for  $E_c = 26 \text{ GPa}$  (3770 ksi),  $K$  is 2.63 and the estimated RF at this particular concrete stiffness is 0.28. Fig. 16 shows the effect of the  $E_c$  on the estimated RF by substituting different values of  $E_c$  in equation (12). The trend of the curve in the Fig. 16 is natural, as an increase in  $E_c$  results in a higher restraining force and higher strain loss; hence decreasing the RF.

The above relationship can be used to determine the variation of the estimated RF over time. This can be done if the development of  $E_c$  over time is known.  $E_c$  can be linked to compressive strength by using equations such as given by Eurocode-2<sup>39</sup> and the development of the compressive strength with time is known from the measurements, as shown in Fig. 17.

Fig. 18 shows the variation of the estimated and apparent RF over time. It can be seen that the apparent RF is higher than the estimated RF (up to 25 days). This may be attributed to that fact that the estimated RF does not include the effect of tensile drying creep/relaxation (partly due to

microcracking) which reduces the tensile stress, resulting in a lower strain loss and consequently higher RF. Once the concrete cracks, the concrete stiffness is reduced and the apparent RF increases temporarily as a consequence.

Fig. 19 shows the variation over time of the ratio of the estimated elastic tensile stress to the instantaneous predicted tensile strength of concrete. The predicted tensile strength is obtained using Eurocode -2 model for development of compressive strength<sup>39</sup>. The tensile stress developed in the concrete is calculated based on the RF, free shrinkage and  $E_c$  (product of :  $RF \times \varepsilon_{free} \times E_c$ ). It can be seen that the developed stress using the estimated RF leads to a lower stress/strength ratio than that of apparent (measured) RF. This may again be attributed to creep effects. A high stress/strength ratio (around 0.75) can also be seen developing at early stages of drying and, this ratio increased to 0.98 at 7 days. This predicts very well the time of development of the first crack, which became visible after 9 days of drying.

## **Compressive Strength**

Almost all previous studies utilized uniaxial compression strength to quantify the effect of drying on concrete mechanical properties. The results of the compressive strength for the water cured cubes (WC/cubes) and portions of prisms (WC/prism) tested in flexural according to BS 1881-119 and the residual compressive strength of the free and restrained specimens at 77 days, are shown in Fig. 20. The result is the average of 3 samples for the cubes and 2 samples for the prisms. The compressive strength (cubes) at 28 days was 52.5 MPa (7613 psi). It can be seen that the compressive strength of the concrete exposed to restrained shrinkage reduced by 19% in comparison to that of WC/prisms and 14% in comparison to the free specimen.

The mechanical properties (strength and stiffness) of concrete may be affected by the drying shrinkage (without external restraint) in two ways. On the one hand, the strength increases as a result of an increase in capillary pressure (which acts as isotropic pressure) on the C-S-H particles when the saturation decreases. This can lead to a stiffening effect by increasing the bonding

between the C-S-H particles<sup>40</sup>. On the other hand, the strength and the stiffness decrease due to the formation of microcracks (which develop due to non-uniform shrinkage, enhanced by local restraint by the aggregates)<sup>40</sup>. In these tests it is clear that shrinkage cracks were dominant in reducing the compressive strength.

### **Flexural strength and flexural elastic modulus ( $E_{fmax}$ )**

The load-deflection curves of water cured specimen, free specimen and restrained shrinkage specimen are shown in Fig. 21. The unrestrained air and water cured specimens behave in a similar manner having similar flexural stiffness around 40 GPa (5800 ksi) and similar strength (free 5.94 MPa, 861 psi and water cured 6.21 MPa, 900 psi). The restrained specimen only reached around 82% (4.89 MPa, 709 psi) of that of unrestrained specimen. This means that the restrained shrinkage induced cracks caused a reduction of around 18% in its flexural capacity. These cracks not only affected the strength, but also reduced the initial stiffness (flexural modulus of elasticity). Fig. 22 shows the estimated flexural modulus of elasticity ( $E_{flex}$ ) against the bending load. The  $E_{fmax}$  of the restrained specimen (31.6 GPa, 4582 psi) is lower than that of both the free shrinkage (40.5 GPa, 5873 psi) and the control specimen (40 GPa, 5800 psi). Restrained shrinkage induced cracks led to around 21% loss in flexural stiffness affecting the stiffness in exactly the same way as the strength.

### **General discussion**

The proposed rig for restraining concrete only provided a variable RF which started at around 0.64 and ended up at around 20%. The drop of RF with time can be explained by the development of the concrete stiffness. The rig managed to provide enough restraint to lead to concrete cracking due to exceedance of the flexural strength around 7 days. More restraint will help (higher degree of restraint is expected to cause earlier cracking), but it is unlikely that the effect on residual stiffness will be great since it is clear that concrete autoheals. Nonetheless, most of the strain loss is a result of rig deformations and an improved rig needs to be developed. To counteract

the change in RF with time, the rig could be prestressed before concrete casting and the stress released as the concrete hardens.

## **CONCLUSIONS**

This paper proposes a new rig and a test procedure to assess the post shrinkage cracking mechanical behaviour of concrete. Results from bending and compression tests showed that restrained shrinkage induced cracks can affect the mechanical behaviour (flexural and compressive strength and flexural stiffness) of concrete by up to 21%. However, this was a very limited proof-of-concept study and more tests are required to validate this conclusion. The proposed rig only provided partial restraint and proposals for improvements are made. The RF was shown to vary with time due to the concrete strength/stiffness evolution and crack development.

## **REFERENCES**

1. ACI 231R-10, "Report on Early-Age Cracking: Causes, Measurement, and Mitigation" ACI committee 231, American Concrete Institute, Farmington Hills, USA, 2010.
2. Carlson RW, "Attempts to Measure the Cracking Tendency of Concrete " ACI Journal, V.36. 1940, pp. 533-537.
3. Hughes BP, "A new look at rigid concrete pavement design," Proceeding of Institution of Civil Eng-Transp, V. 156, No. 1, Feb. 2003, pp. 29-36.
4. Bishop J., "The early age Behaviour of Concrete Industrial Ground Floor Slabs", Doctoral Thesis, Loughborough University, UK, 2001.
5. ACI 207.2R, "Report on Thermal and Volume Change Effects on Cracking of Mass Concrete," ACI committee 207, American Concrete Institute, Farmington Hills, U.S.A, 2002.
6. Banthia N, Gupta R, "Influence of polypropylene fiber geometry on plastic shrinkage cracking in concrete," Cement Concrete Res, V. 36, No. 7. 2006, pp. 1263-7.

7. Bisschop J, Van Mier JGM, "Effect of aggregates on drying shrinkage microcracking in cement-based composites," *Materials and Structures*, V. 35, No. 252 SPEC. 2002, pp. 453-61.
8. Concrete Society TR 34, "Concrete Industrial Ground Floors - A Guide to their Design and Construction," Concrete Society, Surrey, UK, 2003.
9. Grzybowski M, Shah SP, "Model to Predict Cracking in Fiber Reinforced-Concrete Due to Restrained Shrinkage," *Mag Concrete Res*, V. 41, No. 148, Sep. 1989, pp. 125-35.
10. Swamy RN, Stavrides H, "Influence of Fiber Reinforcement on Restrained Shrinkage and Cracking," *of ACI Journal*, V. 76, No. 3. 1979, pp. 443-60.
11. Weiss WJ, Yang W, Shah SP, "Shrinkage cracking of restrained concrete slabs," *J Eng Mech-ASCE*, V. 124, No. 7, Jul. 1998, pp. 765-74.
12. Carlswald J, "Shrinkage Cracking of Steel Fibre Reinforced Self-Compacting Concrete Overlays," Doctoral thesis, Lulea University of Technology, Sweden, 2006.
13. Altoubat SA, Lange DA, "Creep, shrinkage, and cracking of restrained concrete at early age," *ACI Mater J/ SP*, V. 98, No. 4, Jul-Aug. 2001, pp. 323-31.
14. Kovler K, "Testing System for Determining the Mechanical-Behavior of Early Age Concrete under Restrained and Free Uniaxial Shrinkage," *Mater Struct*, V. 27, No.170, Jul. 1994, pp. 324-30.
15. Carlson RW, "Cracking of Concrete," *The Boston Society of Civil Engineers*, V. 29, No. 2. 1942, pp.98-109.
16. Banthia N, Yan C, Mindess S, "Restrained shrinkage cracking in fiber reinforced concrete: A novel test technique," *Cement Concrete Res*, V. 26, No. 1, Jan. 1996, pp. 9-14.
17. Qiao P, McLean, D. and Zhuang, J., "Mitigation Strategies for Early-Age Shrinkage Cracking in Bridge decks" WA-RD Report No. 747, Washington State University, Washington, 2010.
18. Bentur A, Kovler K, "Evaluation of early age cracking characteristics in cementitious systems," *Mater Struct*, V. 36, No. 3, 2003. 2003, pp. 183-90.

19. Bentur A, "Report of RILEM Technical Committee 181-EAS- Early age shrinkage induced stresses and cracking in cementitious system, Benture A., RILEM, 2003, pp. 241-55.
20. Springenschmid R, Breitenbucher, R., Mangold, R., "Development of the cracking frame temperature-stress testing machine," in Thermal Cracking in Concrete at Early Ages, RILEM, E&FN SPON, 1994, pp. 137-44.
21. JCI, "Technical Committee on Autogenous Shrinkage of Concrete " Report: Workshop on Autogenous Shrinkage of Concrete, Japan Concrete Institute, Japan, 1998, pp. 5-66.
22. Collins F, Sanjayan JG, "Cracking tendency of alkali-activated slag concrete subjected to restrained shrinkage," Cement Concrete Res, V. 30, No. 5, May. 2000, pp. 791-8.
23. Bloom R, Bentur A, "Free and Restrained Shrinkage of Normal and High-Strength Concretes," ACI Mater J, V. 92, No. 2, Mar-Apr. 1995, pp. 211-7.
24. Springenschmidt R, "Prevention of Thermal Cracking in Concrete at Early Ages-State of the Art Report" London:E&FN Spon; 1998.
25. Paillere A. M. BM, Serrano J. J., "Effect of Fiber Addition on the Autogenous Shrinkage of Silica Fume," ACI Mater J, V. 86, No. 2, 1989, pp. 6.
26. Igarashi S, Bentur A, Kovler K, "Autogenous shrinkage and induced restraining stresses in high-strength concretes," Cement Concrete Res, V. 30, No. 11, Nov. 2000, pp. 1701-7.
27. Banthia N, Azzabi M, Pigeon M, "Restrained Shrinkage Cracking in Fiber-Reinforced Cementitious Composites," Mater Struct, V. 26, No. 161, Aug-Sep. 1993, pp. 405-13.
28. Leung CKY, Asce M, Lee AYP, Lai R, "A new testing configuration for shrinkage cracking of shotcrete and fiber reinforced shotcrete," Cement Concrete Res, V. 36, No. 4. 2006, pp. 740-8.
29. Hossain AB, and Weiss, W. J. "Assessing Residual Stress Development and Stress Relaxation in Restrained Concrete Ring Specimens," Cement and Concrete Composites, V. 26. 2004, pp. 531-40.

30. BS EN 197-1:2011, "Cement. Composition, specifications and conformity criteria for common cements," British Standard Institution, London, UK, 2011.
31. ACI 207.2R-95, "Effect of Restraint, Volume Change, and Reinforcement on Cracking of Mass Concrete," American Concrete Institute, Farmington Hills,U.S.A, 1995, pp. 47.
32. Abbasnia R, Godossi P, Ahmadi J, "Prediction of restrained shrinkage based on restraint factors in patching repair mortar,"Cement Concrete Res, V. 35, No.10, Oct.2005, pp. 1909-13.
33. Idiart AE, "Coupled analysis of degradation processes in concrete specimens at the meso-level," Doctoral thesis, Polytechnic University of Catalunya, Barcelona, Spain, 2009.
34. Bisschop Jan, "Drying Shrinkage Microcracking in Cement-based Materials,"Doctoral Thesis, Delft University of Technology, Delft, Netherland, 2002.
35. Shiotani T, Bisschop J, Van Mier JGM, "Temporal and spatial development of drying shrinkage cracking in cement-based materials," Eng. Fracture Mechanics, V. 70, No. 12. 2003, pp. 1509-25.
36. BS EN 12390-3:2009, "Testing hardened concrete Part 3: Compressive strength of test specimens," British Standards Institution, London, UK, 2009.
37. BS 1881-119:2011, "Testing concrete. Method for determination of compressive strength using portions of beams broken in flexure" British Standards Institution, London , UK, 2011, pp. 12.
38. ASTM C1609/C1609M-12, "Standard Test Method for Flexural Performance of Fiber-Reinforced Concrete (Using Beamwith Third-Point Loading)", ASTM International, 2012.
39. BS EN 1992-1-1:2004, "Eurocode 2: Design of concrete structures-Part 1-1:General rules and rules for buildings " British Standard Institution, London, UK, 2004.
40. Yurtdas I, Peng H, Burlion N, Skoczylas F, "Influences of water by cement ratio on mechanical properties of mortars submitted to drying," Cement Concrete Res, V. 36, No.7. 2006, pp.1286-93.

## **Tables and Figures**

### **List of Tables**

Table 1 Cracking time and width and length of cracks.

## List of Figures

Figure 1 Ring test apparatus.

Figure 2 (a-c) Schematics of previously attempted configurations to simulate restrained shrinkage, (d-f) End gripping arrangements.

Figure 3 Geometry of the restraining rig used by Weiss et al. (1998)

Figure 4 Front view of the developed rig for restrained shrinkage test (Note 1 mm= 0.04 in).

Figure 5 Distribution of Demec points for restrained specimen.

Figure 6 Free shrinkage strains of the side surface.

Figure 7 Free shrinkage strain of the top surface.

Figure 8 Shrinkage strains of the restrained sample using 50 mm gauge length.

Figure 9 Shrinkage strains of the restrained specimen using 300 mm gauge length.

Figure 10 RF calculated from the strains measured (on the side of the specimen) using 300 mm gauge length.

Figure 11 Crack distribution at day 75 on the sides of the restrained specimen.

Figure 12 a-Evolution of mass loss of the free sample, b- Mass loss against shrinkage strain.

Figure 13 Schematic representation the deformations of the rig caused by the restrained shrinkage of concrete.

Figure 14 Finite element analysis a-stresses , b- strains.

Figure 15 Shrinkage induced strains (deformations) in concrete and rig.

Figure 16 Effect of elastic modulus of concrete ( $E_c$ ) on the estimated RF (Note 1 GPa= 145 ksi).

Figure 17 Development of compressive strength (Note 1 MPa= 145 psi).

Figure 18 Variation of estimated and measured RF over time.

Figure 19 Variation of stress/strength ratio over time.

Figure 20 Results of compressive strength.

Figure 21 Mid -span deflection versus bending load.

Figure 22 Flexural elastic modulus ( $E_{flex}$ ) versus bending load (Note: 1 kN = 0.2248lb, 1GPa = 145 ksi).

Table 1 Cracking time and width and length of cracks.

Crack code	Drying time (day)*	Crack width, mm (in)		Crack length, mm (in)	
		Initial	Final **	Initial	Final ***
1	9	0.025 ( $1 \times 10^{-3}$ )	0.055 ( $2.2 \times 10^{-3}$ )	15 (0.6)	43 (1.7)

2	9	0.025 ( $1 \times 10^{-3}$ )	0.035 ( $1.4 \times 10^{-3}$ )	12 (0.5)	32 (1.3)
3	9	0.025 ( $1 \times 10^{-3}$ )	0.045 ( $1.8 \times 10^{-3}$ )	10 (0.4)	35 (1.4)
4	9	0.025 ( $1 \times 10^{-3}$ )	0.04 ( $1.6 \times 10^{-3}$ )	12 (0.5)	30 (1.2)
5	10	0.035 ( $1.4 \times 10^{-3}$ )	0.045 ( $1.8 \times 10^{-3}$ )	11 (0.44)	38 (1.5)
6	11	0.025 ( $1 \times 10^{-3}$ )	0.04 ( $1.6 \times 10^{-3}$ )	11 (0.44)	25 (1.0)
7	11	0.025 ( $1 \times 10^{-3}$ )	0.04 ( $1.6 \times 10^{-3}$ )	12 (0.5)	28 (1.1)
8	11	0.025 ( $1 \times 10^{-3}$ )	0.045 ( $1.8 \times 10^{-3}$ )	12 (0.5)	30 (1.2)
9	11	0.02 ( $8 \times 10^{-4}$ )	0.04 ( $1.6 \times 10^{-3}$ )	12 (0.5)	33 (1.3)
10	11	0.02 ( $8 \times 10^{-4}$ )	0.04 ( $1.6 \times 10^{-3}$ )	11 (0.44)	30 (1.2)

\* Drying time when the crack is visible. \*\* Crack width at age 75 days. \*\*\* Crack length at age 75 days.

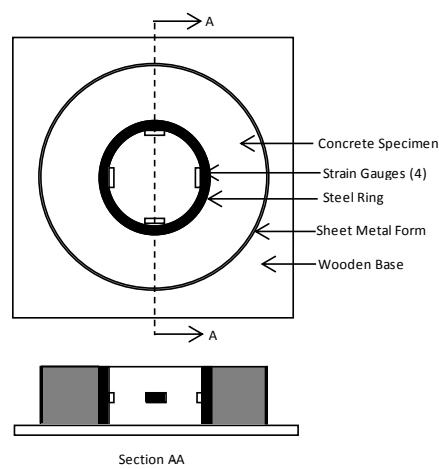


Fig. 1- Ring test apparatus.

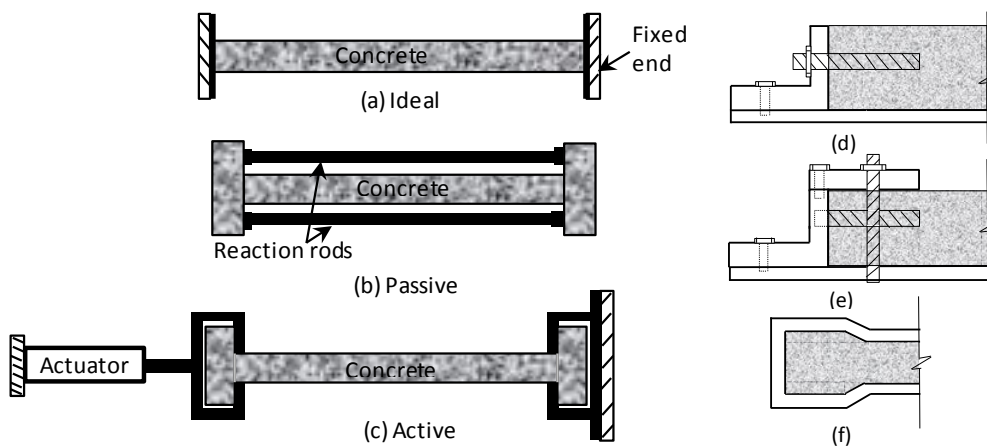


Fig. 2- (a-c) Schematics of previously attempted configurations to simulate restrained shrinkage, (d-f) End gripping arrangements.

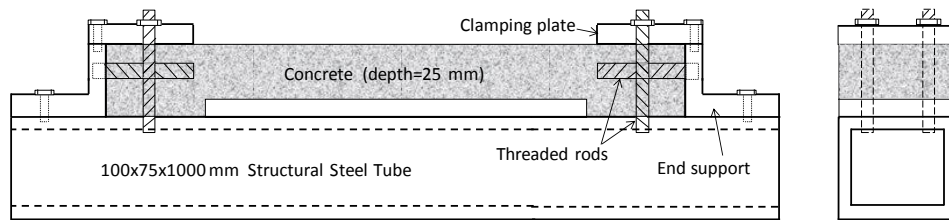


Fig. 3- Geometry of the restraining rig used by Weiss et al.<sup>11</sup>

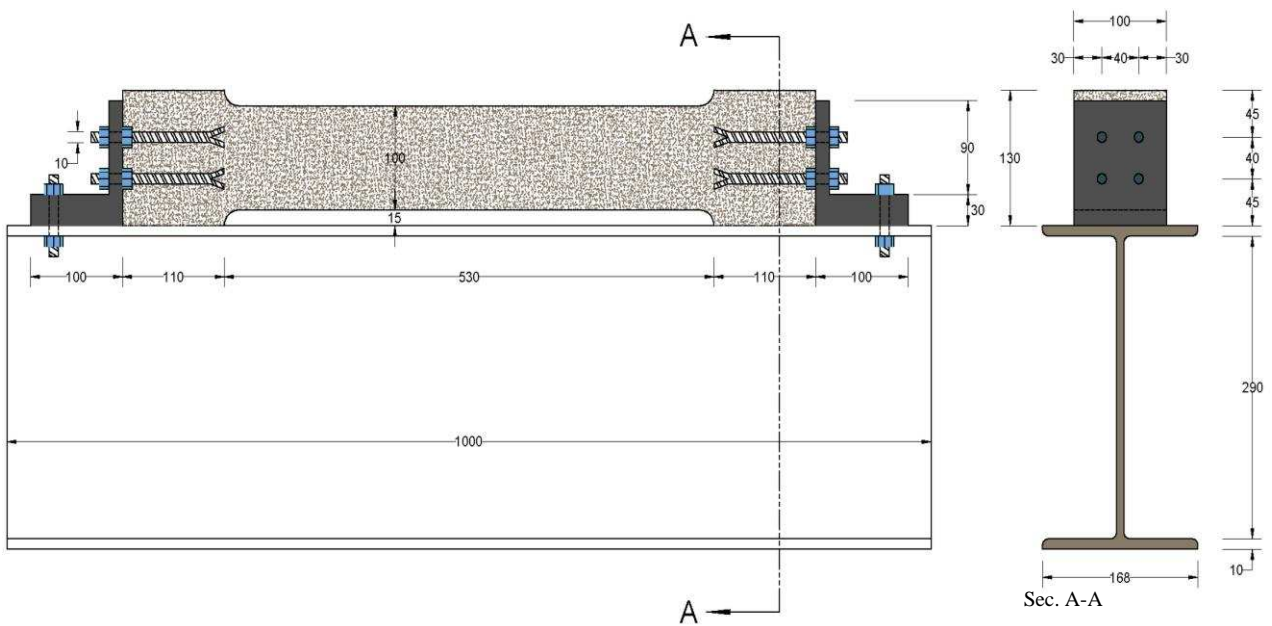


Fig. 4- Front view of the developed rig for restrained shrinkage test, all dimensions in mm ( Note 1 in= 25.4 mm).

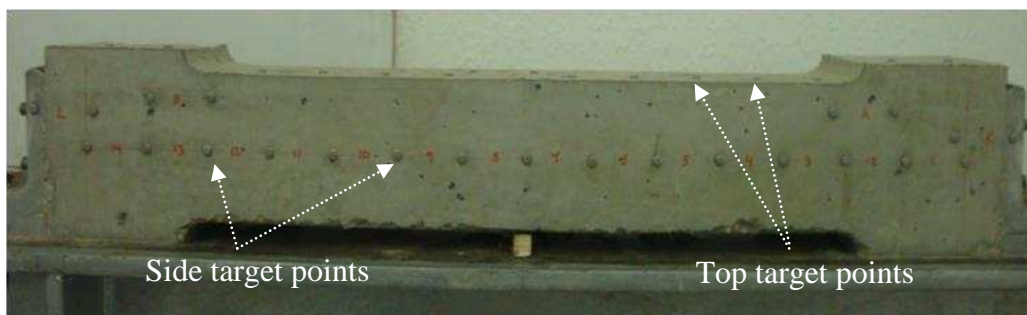


Fig. 5- Distribution of Demec points for restrained specimen.

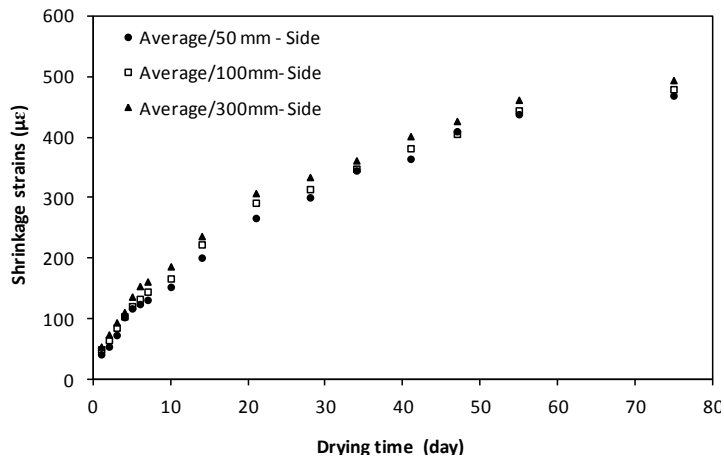


Fig. 6- Free shrinkage strains of the side surface.

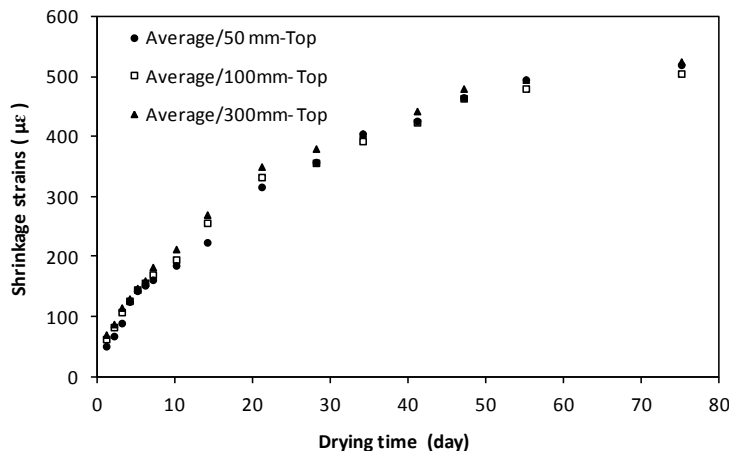


Fig. 7- Free shrinkage strain of the top surface.

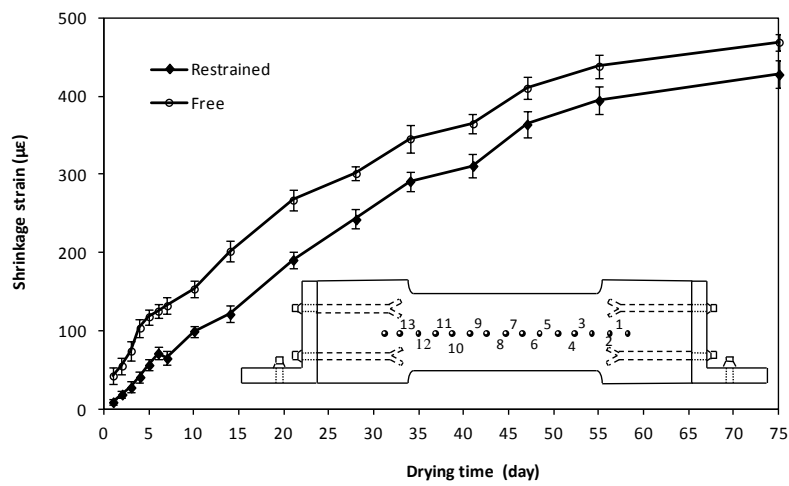


Fig. 8- Shrinkage strains of the restrained sample using 50 mm gauge length.

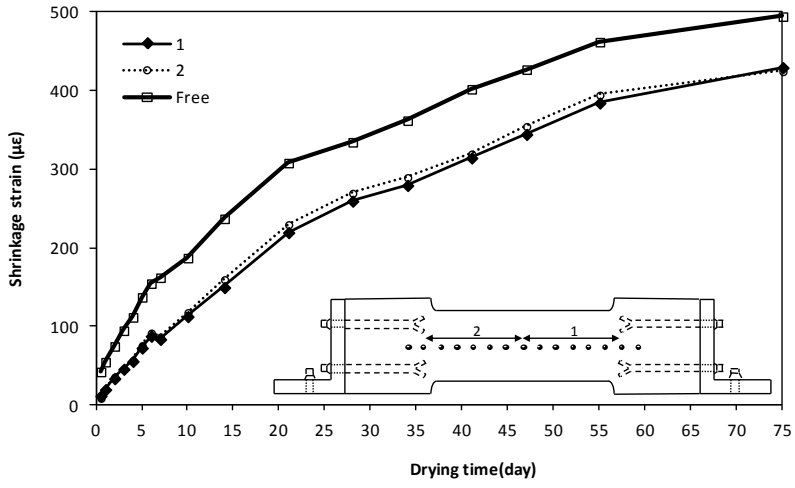


Fig. 9- Shrinkage strains of the restrained specimen using 300 mm gauge length.

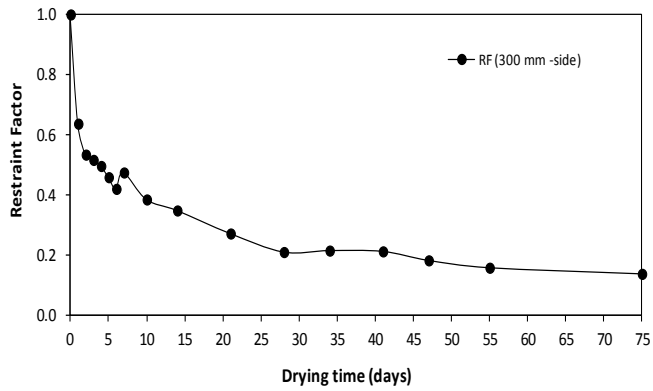


Fig. 10-RF calculated from the strains measured (on the side of the specimen) using 300 mm gauge length.

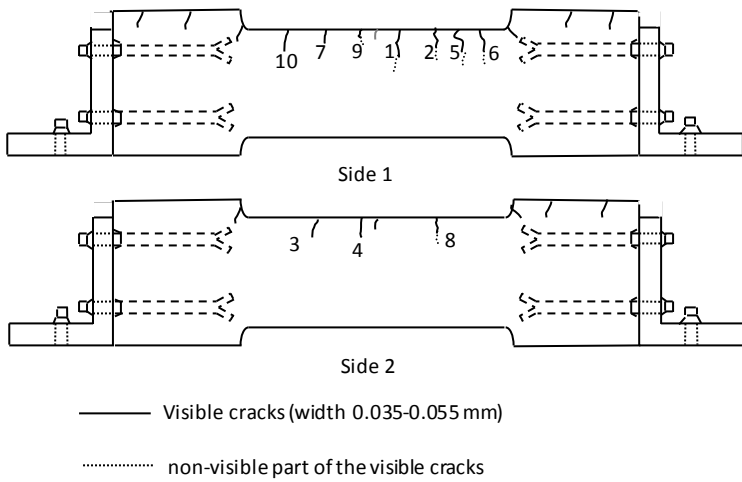


Fig. 11-Crack distribution at day 75 on the sides of the restrained specimen (1mm =0.04in).

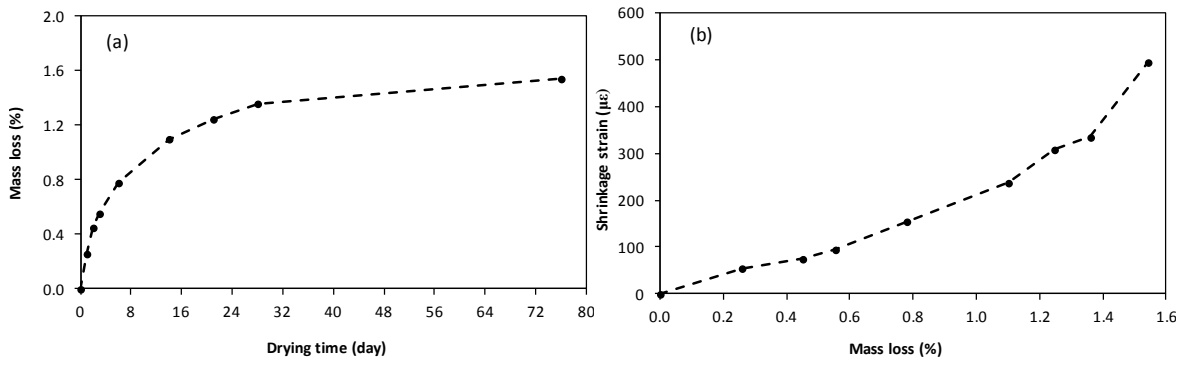


Fig. 12- a-Evolution of mass loss of the free sample, b- Mass loss against shrinkage strain



Fig. 13- Schematic representation the deformations of the rig caused by the restrained shrinkage of concrete.

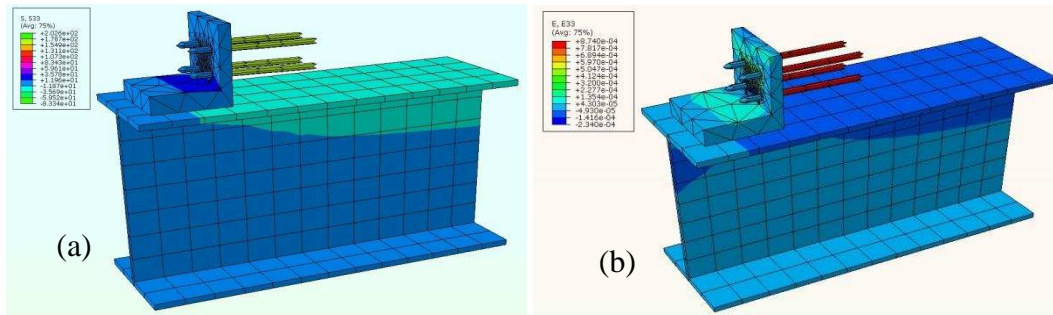


Fig.14- Finite element analysis a-stresses , b- strains.

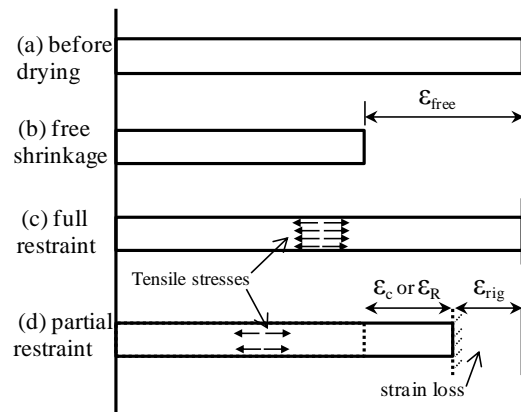


Fig. 15-Shrinkage induced strains (deformations) in concrete and rig.

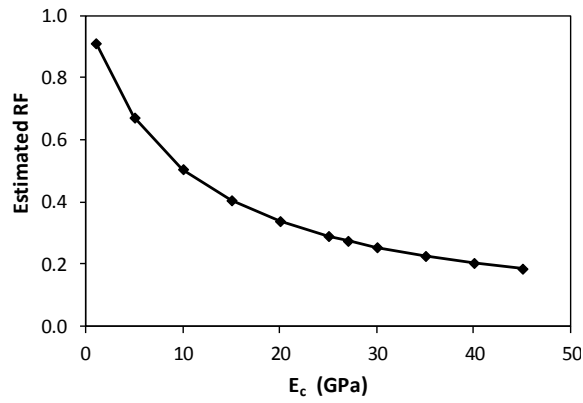


Fig. 16- Effect of elastic modulus of concrete ( $E_c$ ) on the estimated RF (Note: 1 GPa = 145 ksi).

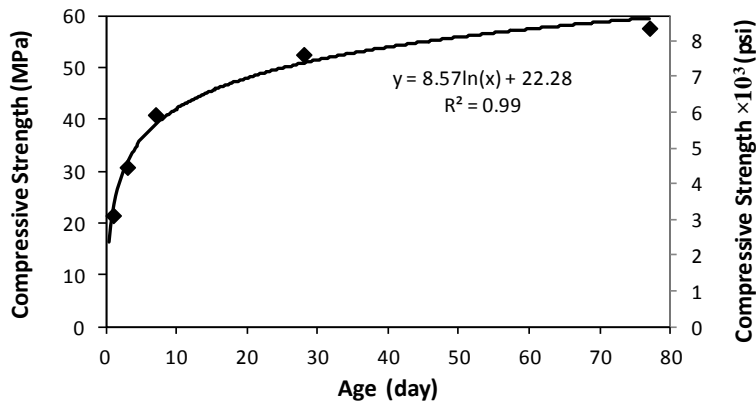


Fig. 17- Development of compressive strength (Note: 1 MPa = 145 psi).

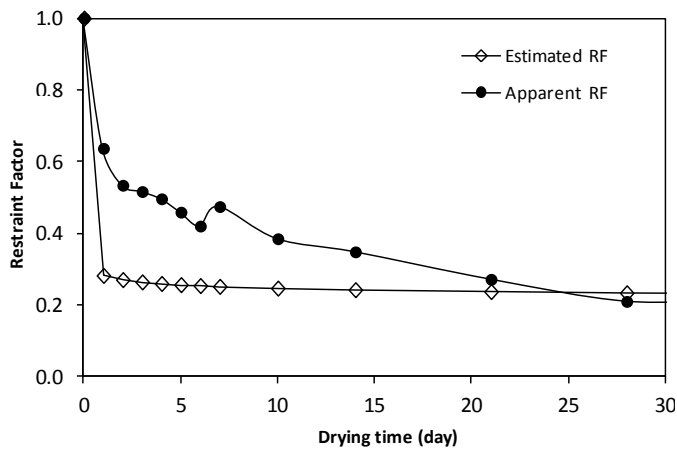


Fig. 18- Variation of estimated and measured RF over time.

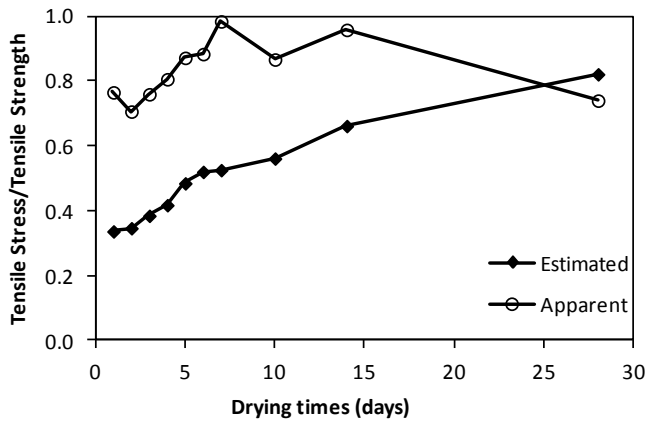


Fig. 19- Variation of stress/strength ratio over time.

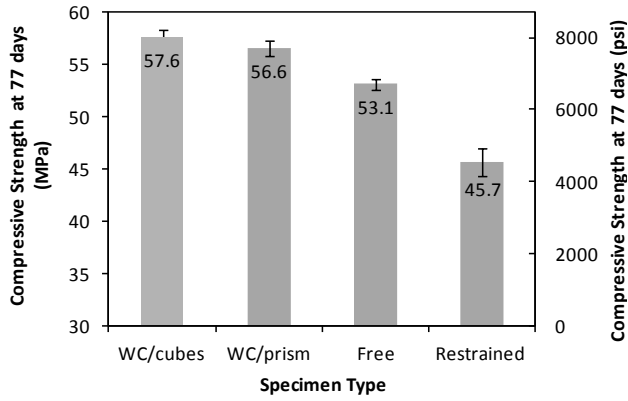


Fig. 20- Results of compressive strength.

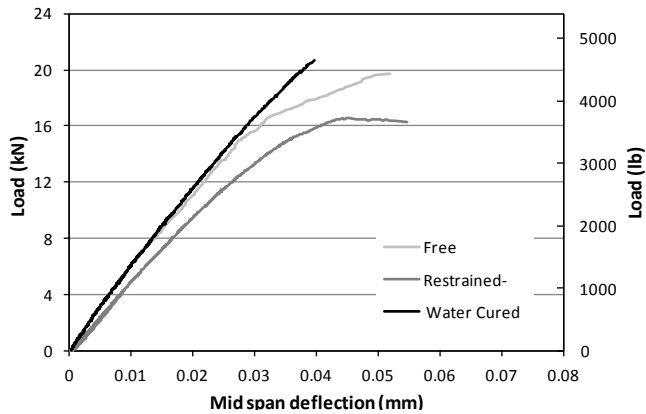


Fig. 21- Mid -span deflection versus bending load (Note: 1 kN=0.2248lb, 1mm = 0.04 in).

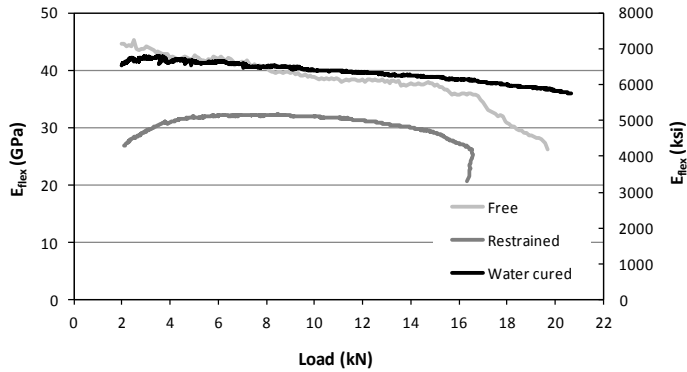


Fig. 22- Flexural elastic modulus ( $E_{flex}$ ) versus bending load (Note: 1 kN = 0.2248lb, 1GPa = 145 ksi).